



# Laboratory Investigation on Shear Behaviors of Bolt–Grout Interface Subjected to Constant Normal Stiffness

Chuanqing Zhang<sup>1,2</sup> · Guojian Cui<sup>1,2</sup> · Liang Deng<sup>3</sup> · Hui Zhou<sup>1,2</sup> · Jingjing Lu<sup>1,2</sup> · Feng Dai<sup>4</sup>

Received: 16 January 2019 / Accepted: 23 September 2019 / Published online: 4 October 2019  
© Springer-Verlag GmbH Austria, part of Springer Nature 2019

## Abstract

Shear behavior of the bolt–grout interface basically depends on site-specific boundary conditions, i.e., initial normal stress and normal stiffness of the borehole wall. Few studies have been conducted to investigate the shear behaviors between the bolt and grout material under different boundary conditions. To better understand the effect of boundary conditions on the shear behaviors of the bolt–grout interface, simplified two-dimensional (2D) bolt–grout interface specimens are prepared and tested using direct shear tests at various initial normal stresses and normal stiffnesses in this context. The testing results showed that both initial normal stress and normal stiffness significantly influence the bolt–grout interface shearing behaviors. Increasing the normal stiffness or initial normal stress would increase the peak and residual shear strength. However, the degree of the brittleness after the peak, normal displacement, and peak friction coefficient was reduced. It is noted that the peak and residual shear strength points under the constant normal stiffness conditions located near the peak and residual strength envelopes for the constant normal load tests, respectively. Besides, the shear failure process of the bolt–grout interface was captured by PAC acoustic emission (AE) monitoring and digital camera technology, a good correlation between the evolution of AE parameters and the shear stress curves was obtained.

**Keywords** Bolt–grout interface · Direct shear test · Constant normal stiffness · Failure mode · Rock bolt

## List of Symbols

2D	Two-dimensional
CNL	Constant normal load
CNS	Constant normal stiffness
AE	Acoustic emission
UCS	Uniaxial compressive strength
$\sigma_{n0}$	Initial normal stress applied on the bolt–grout interface

$k_n$	Normal stiffness applied on the bolt–grout interface
$\sigma$	Normal stress on the bolt–grout interface
$v$	Normal displacement of the bolt–grout interface
$R^2$	Coefficient of determination of the fitting curve

## 1 Introduction

Bolts, a means to improve the geomaterial performances, are widely used in various field applications in the world. The fully encapsulated grouted bolts are basically considered as a reliable and efficient reinforcement method, which have been generally used in civil, tunneling, and mining engineering (Cai et al. 2004; Ma et al. 2013; Li et al. 2016; Salcher and Bertuzzi 2018; Stille et al. 1989; Villaescusa et al. 2008). Results show that the load-bearing capacity and deformation capacity of the fully grouted bolts mainly depend on the shear behaviors of the bolt–grout interface when failure of the rock bolting system occurs at the interface (Thenevin et al. 2017; Chen et al. 2018). In this regard, it is of great significance to study the shear behaviors of the bolt–grout

✉ Guojian Cui  
cgj921211@gmail.com

<sup>1</sup> State Key Laboratory of Geomechanics and Geotechnical Engineering, Institute of Rock and Soil Mechanics, Chinese Academy of Sciences, Wuhan 430071, People's Republic of China

<sup>2</sup> University of Chinese Academy of Sciences, Beijing 100049, People's Republic of China

<sup>3</sup> College of Civil Engineering and Architecture, China Three Gorges University, Yichang 443002, People's Republic of China

<sup>4</sup> State Key Laboratory of Hydraulics and Mountain River Engineering, Sichuan University, Chengdu 610065, Sichuan, People's Republic of China

interface for better understanding the load transfer mechanism of the rock bolting system.

The shear behavior of the bolt–grout interface can be generally determined using the conventional pull- and push-out tests or direct shear tests (Hyett et al. 1992; Aziz 2001; Moosavi et al. 2002; Aziz et al. 2008; Yokota et al. 2018; Zhang et al. 2018). A comparison of these test methods was conducted as listed in Table 1. Conventional pull-out tests are the most commonly used testing methods for rock bolts in geotechnical engineering and can be generally divided into two types according to boundary conditions, i.e., constant radial pressure and constant radial stiffness. A large number of laboratory pull-out tests have been carried out under both boundary conditions (Hyett et al. 1995; Moosavi et al. 2002; Li 2012; Martin 2012; Aziz et al. 2016; Chen et al. 2016). The results suggest that both radial pressure and radial stiffness applied on the bolt–grout interface have a marked influence on the interface shear behaviors.

Moosavi et al. (2005) experimentally studied the effect of confining stress on the bond capacity and revealed that higher bond capacities and lower generated dilations have a close relation with higher confining stress applied. However, constant radial pressure boundary conditions may not reflect the true in situ applications as the changes in the radial stress on the outer surface of cement annulus that resulted from dilation induced by the radial constraint of surrounding rock masses are ignored. For the bolt–grout interface, the normal stress during the shearing depends on the initial radial stress, radial stiffness, and dilation. Therefore, constant radial stiffness boundary condition can better simulate the interface behavior between the bolt and grout material in the field when compared with constant radial pressure boundary condition.

Concerning the constant radial stiffness boundary conditions, Hyett et al. (1992) investigated some major factors influencing the bond capacity of grouted cable bolts using constant radial stiffness pull-out tests. Their results indicate that the radial stiffness acting on the outer surface of the cement annulus is one of the key factors controlling the bond capacity of the rock bolting system. However, it should be noticed that the effect of the initial radial stress is not considered in their tests. In other words, it is rather difficult to accurately apply initial radial stress and radial stiffness simultaneously using conventional pull-out tests. To address this problem, Martin (2012) developed a new pull-out bench to study the bolt–grout interface behavior under both boundary conditions experimentally, i.e., constant radial pressure and constant radial stiffness boundaries. In their tests, constant stiffness conditions were realized by closing the biaxial cell and keeping the confining fluid volume constant.

In laboratory tests, it is basically easier to conduct push-out tests than pull-out tests when using uniaxial compression test system, as the compression load is easier

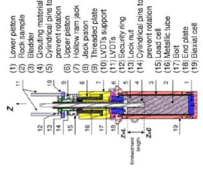
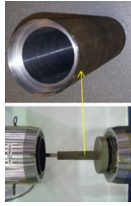

to realize than tensile load does. The push-out test can be considered as an alternative approach when determining the effects of various parameters on the mechanical behavior of the rock bolting system, to investigate the bolt–grout–rock interaction under axial loading (Cao et al. 2013). However, it is noted that the stress state of the bolt in the push-out tests is different from that in the field, resulting in larger load capacity in the push-out test than that in the pull-out test due to the Poisson's ratio effect (Jalalifar 2006; Aziz et al. 2008).

For both pull- and push-out tests, the controlled constant stiffness boundary conditions are not well included. Moreover, the evolution process of damage and failure of the bolt–grout interface is rather difficult to capture due to the encapsulated structure. Therefore, it is not easy to directly measure the radial displacement and radial pressure of the bolt–grout interface. To solve the above problems, the direct shear test is used (Aziz et al. 2001; Cao 2013; Jiang et al. 2016). Aziz et al. (2001) first adopted CNS direct shear tests on the bolt–grout interface. In their study, a normal stiffness of 8.5 kN/mm and initial normal stresses of 0.1–7.5 MPa were applied on the bolt–grout interface to study the load transfer mechanisms of the fully grouted bolt by opening up the bolt surface. The test results suggest that the bolt with deeper rib could offer a higher shear resistance at low normal stress conditions, while the bolts with closer rib spacing offer a higher shear resistance at high normal stress conditions. Cao (2013) used a simplified steel plate to represent a round bolt opened onto a flat plane under the CNS shear testing. It is reported that the failure modes are significantly varied for different bolt profiles, even in one test setup. Parallel shear failure and dilational slip failure could be possible as the major factors accounting for the deformation.

In rock-socketed piles associated with rock joints, CNS direct shear tests have also been conducted to investigate the interface shear behavior (Benmokrane et al. 1994; Indraratna and Haque 2000; Seidel and Haberfield 2002; Jiang et al. 2006; Shrivastava and Rao 2018). It is well acknowledged that boundary conditions can significantly influence the shear failure mechanism and shear behavior. Gu et al. (2003) showed that the normal stiffness has a significant effect on the peak shear strength, and wear at the rock–concrete interface increases with an increase in either normal stiffness or initial normal stress values.

To better understand the shear behavior and failure process of the bolt–grout interface, CNS direct shear tests under different initial normal stresses and normal stiffnesses were carried out in this context. The shear behaviors under different boundary conditions were studied and the variation of the shear parameters with either normal stiffness or initial normal stress was analyzed. Finally, acoustic emission (AE) and digital video camera were used to evaluate the interface damage during the shearing

**Table 1** Comparison of three commonly used test methods for the bolt–grout interface shearing

No.	Method	Boundary conditions	Advantages	Disadvantages	Example
1	Pull-out test	Constant radial pressure or constant radial stiffness	The bolt is in tension and can reflect true load transfer mechanism similar to in situ conditions (anchor length); can measure the load capacity of the rock bolt; axisymmetric structure	Failure process is hard to be revealed; the effect of radial stiffness and the confining pressure is ignored in the constant radial pressure and constant radial stiffness tests, respectively; test variables are difficult to change, especially for constant radial stiffness tests; lateral displacement and interface pressure are difficultly measured; specimen preparation process is complex; the pull-out test equipment is essential	 <p>Martin (2012)</p>
2	Push-out test	Constant radial stiffness	The test can be performed easily using universal equipment such as uniaxial test system	Failure process is also hard to be revealed; the effect of the confining pressure is ignored; lateral displacement and interface pressure are difficultly measured; specimen preparation process is complex; cannot reflect the true load transfer capability due to the bolt is in compression	 <p>Aziz et al. (2016)</p>
3	Direct shear test	Constant normal stress or constant normal stiffness	Failure process can be evaluated; test variables can be easily controlled; the specimens can be cast easily; the dilation and normal stress can be directly measured	CNS direct shear test equipment is essential; the bolt profiles must be simplified; cannot study the true load transfer mechanism of bolting system; the stress state of grout during shearing is different from that during pulling out due to two-dimension structure	 <p>Indraratna et al. (1998)</p>

process. The correlation between shear behavior and AE characteristics was also discussed.

## 2 Sample Preparation and Experimental Set-up

### 2.1 Sample Preparation

As the roughness of the bolt–grout interface can influence the interface shear behavior dramatically, the bolt profiles should be first determined. In this study, a 100-mm long steel plate was used to model the rock bolt, the profiles of steel plate were designed in accordance with the specification of a type of threadbar used in China. The transverse rib of rock bolt is simplified as isosceles trapezoid rib in the steel plate with rib top width of 2.5 mm, rib base width of 4.5 mm, and rib height of 1.2 mm. The rib face angle is set at  $90^\circ$  for simplicity and the rib spacing is 10 mm based on the bolt prototype. The simplified steel plate is shown in Fig. 1.

When preparing grout specimens, the steel plate was first placed in a steel mold with a dimension of 100 mm  $\times$  100 mm  $\times$  50 mm (length  $\times$  width  $\times$  height). Then the mixture of cement (32.5 R), sand, tap water, and early strength agent of calcium formate at a ratio of 1:1:0.4:0.03 by weight was cast into the steel mold and then was vibrated for 1 min to eliminate air bubbles. The grout specimens were removed from the molds in 24 h and finally were cured in a concrete curing box in room temperature ( $20 \pm 1$ )  $^\circ\text{C}$  and humidity of no less than 95% for 3 days before conducting CNS direct shear tests. Uniaxial compression test was used to estimate the mechanical properties of grout material. The testing results show that the uniaxial compressive strength (UCS), Young's

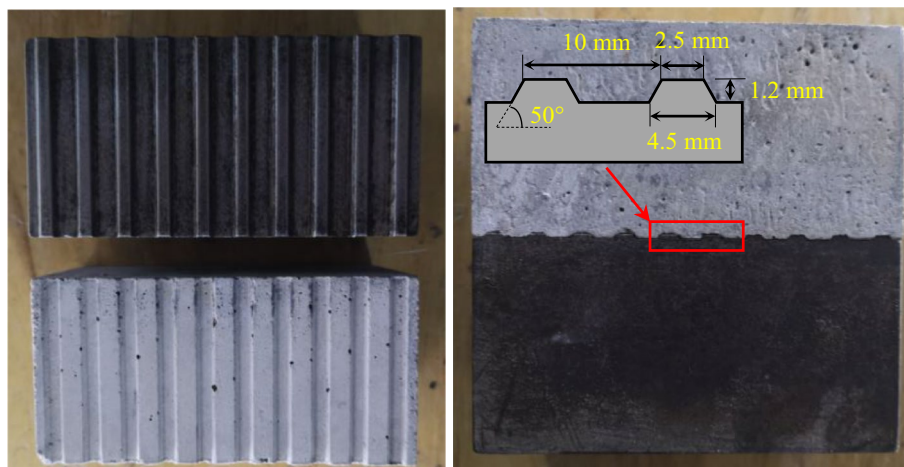
modulus, and Poisson's ratio of grout specimens are 29.64 MPa, 7.54 GPa, and 0.25, respectively.

### 2.2 Experiment Set-up

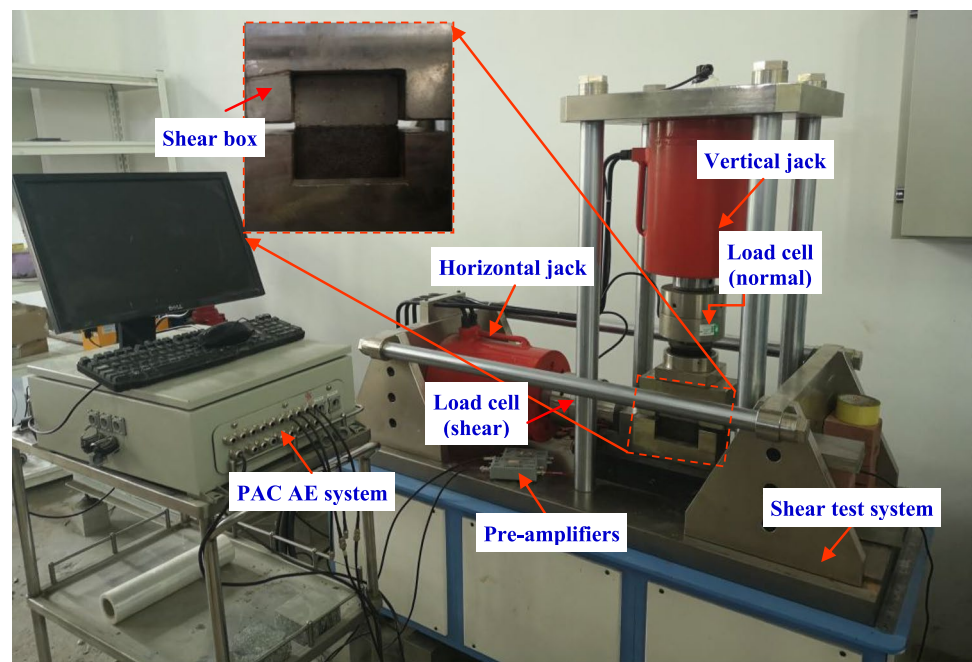
A servo-controlled rock joint direct shear test apparatus (Model RJST-616, Fig. 2a), which was developed in Institute of Rock and Soil Mechanics, Chinese Academy of Sciences (CAS), was used to conduct bolt–grout interface direct shear tests under both CNL and CNS boundaries. The shear test apparatus consists of data acquisition and controlling system, hydraulic power system, vertical loading system (normal loading) and horizontal loading system (shear loading) with loading capacities of 200 kN and 300 kN, respectively. The upper shear box was fixed in the horizontal direction and can only move along the vertical direction. The lower box is placed in a linear guideway and can move merely along the horizontal direction. Therefore, the apparatus ensures that the lower specimen only moves along the horizontal direction and upper specimen only along the vertical direction. The normal and shear loads were recorded in real time by load cells connected to the vertical and horizontal hydraulic jacks, respectively. The normal displacement was measured by a built-in magnetostrictive displacement transducer and shear displacement was measured by a linear variable differential transformer (LVDT) having an accuracy of  $\pm 0.001$  mm. Both normal and shear loads can be programmed and applied by either load or displacement rate control mode. The CNS boundary condition was achieved by feedback hydraulic servo-controlled system. The normal stiffness  $k_n$  can be set in the range of 1–1000 GPa/m when the dimension of the shear plane is 50 mm  $\times$  100 mm.

The PAC AE system and a digital video camera were also used to visualize the shear failure process of the bolt–grout interface. A Nano-30 miniature AE sensor was attached to a steel plate before the shear test. It has a resonant response at 300 kHz and good frequency response over the range of

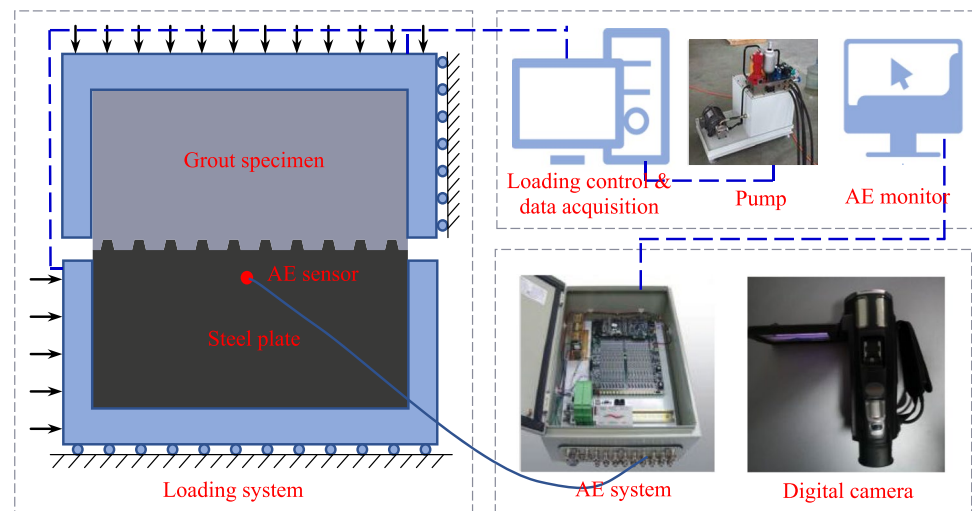
**Fig. 1** Simplified steel plate and grout specimen



**Fig. 2** Arrangement of the CNS direct shear test: **a** shear test system and PAC AE system; **b** schematic view of the loading test system layout



(a)



(b)

125–750 kHz. The AE parameters, such as energy rate and hit rate, were recorded, and the images of the damage evolution process on the surface of the bolt–grout specimens were captured during the shearing process. In addition, amplification of the preamplifier was set at 40 dB. The acquisition frame rate of the digital video camera used in the text is 20 Hz.

### 2.3 Experiment Scheme and Test Procedure

Similar to the radial boundary conditions in conventional pull-out tests, direct shear tests of the bolt–grout interface were conducted under both CNL and CNS conditions. In the

direct shear tests, the initial normal stresses are set at 0.5, 1, and 2 MPa because the actual radial stress generated on the bolt–grout interface is generally small resulting from grouting pressure and redistributed stress before surrounding rock masses deform. After the initial normal stress is reached, constant normal stress or constant normal stiffness condition is applied on the bolt–grout interface, which depends on the prescribed boundary conditions. For the CNS tests, the normal stiffnesses are set at 10, 50, 100, 200, and 400 GPa/m in this study. Based on the field measurement results reported by Hyett et al. (1992), the applied stiffnesses were found to be representatives of the surrounding rock mass conditions from soft coal rock to weathered granite. It should be noted

**Table 2** Direct shear test designs for the bolt–grout interface

Test conditions	Initial normal stress (MPa)	Normal stiffness (GPa/m)
CNL	0.10, 0.25, 0.50, 1.00, 2.00, 5.00	0.00
CNS	0.50, 1.00, 2.00	10.00, 50.00, 100.00, 200.00, 400.00

that the applied normal stiffnesses are not large enough to simulate harder rocks such as limestone and fine granite. For this, the associated test facility needs to be improved with respect to testing of harder rocks in the future. Moreover, additional CNL shear tests under normal stresses of 0.1, 0.25, and 5 MPa were performed to obtain CNL strength envelope, to compare the relationship between the CNL strength envelope and CNS peak stress points, due to the varied normal stress on the bolt–grout interface during the CNS tests. A summary of the experiment schemes is given in Table 2.

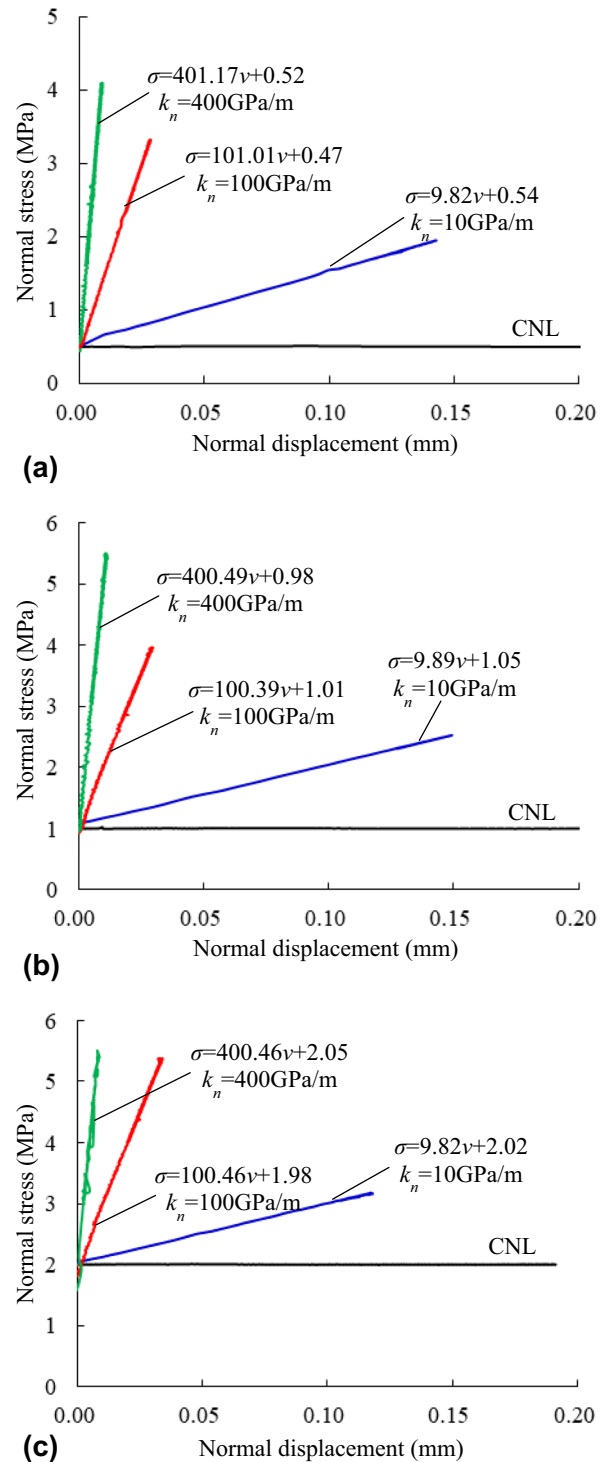
During the direct shear tests, the bolt–grout specimen was placed inside the shear box. Followed by either constant normal load or constant normal stiffness condition was maintained on the bolt–grout interface until the end of the shear tests, accompanied by shear loading. The initial normal stress was first applied on the upper shear box at a loading rate of 0.1 kN/mm, and then the shear load was applied on the lower shear box at shear velocity of 0.005 mm/s. The shear test was terminated when the shear displacement exceeded 6 mm.

### 3 Results

#### 3.1 Shear Behavior of the Bolt–Grout Interface in the CNS Tests

The shear behaviors of the bolt–grout interface under the initial normal stress of 0.5–2 MPa and normal stiffnesses of 0–400 GPa/m are shown in Figs. 3, 4 and 5. The results reveal that the normal stiffness can influence the mechanical behaviors and deformation of the bolt–grout interface.

Figure 3 depicts the relationships between the normal stress and normal displacement during the shearing process under both CNL and CNS conditions. As can be observed, the normal stress kept constant in the CNL test and increased linearly with increasing normal displacement in the CNS tests. Taking the results at the initial normal stress of 0.5 MPa as an example, the fitting linear regression formulas



**Fig. 3** Normal stress versus normal displacement curves under the normal stiffnesses of 0, 10, 100, and 400 GPa/m and respective fitting linear regression formulas: **a**  $\sigma_{n0} = 0.5$  MPa; **b**  $\sigma_{n0} = 1.0$  MPa; **c**  $\sigma_{n0} = 2.0$  MPa

of the normal stress versus normal displacement curves under the CNS conditions can be expressed as follows:

For normal stiffness of 10 GPa/m:

**Fig. 4** Curves of shear behavior for the bolt–grout interface under the initial normal stress of 0.5 MPa and normal stiffnesses of 0, 10, 100, and 400 GPa/m: **a** shear stress versus shear displacement curves; **b** friction coefficient versus shear displacement curves; **c** normal displacement versus shear displacement curves; and **d** normal stress versus shear displacement curves

$$\sigma = 9.82v + 0.54(R^2 = 1.00) \tag{1}$$

For normal stiffness of 100 GPa/m:

$$\sigma = 101.01v + 0.47(R^2 = 1.00) \tag{2}$$

For normal stiffness of 400 GPa/m:

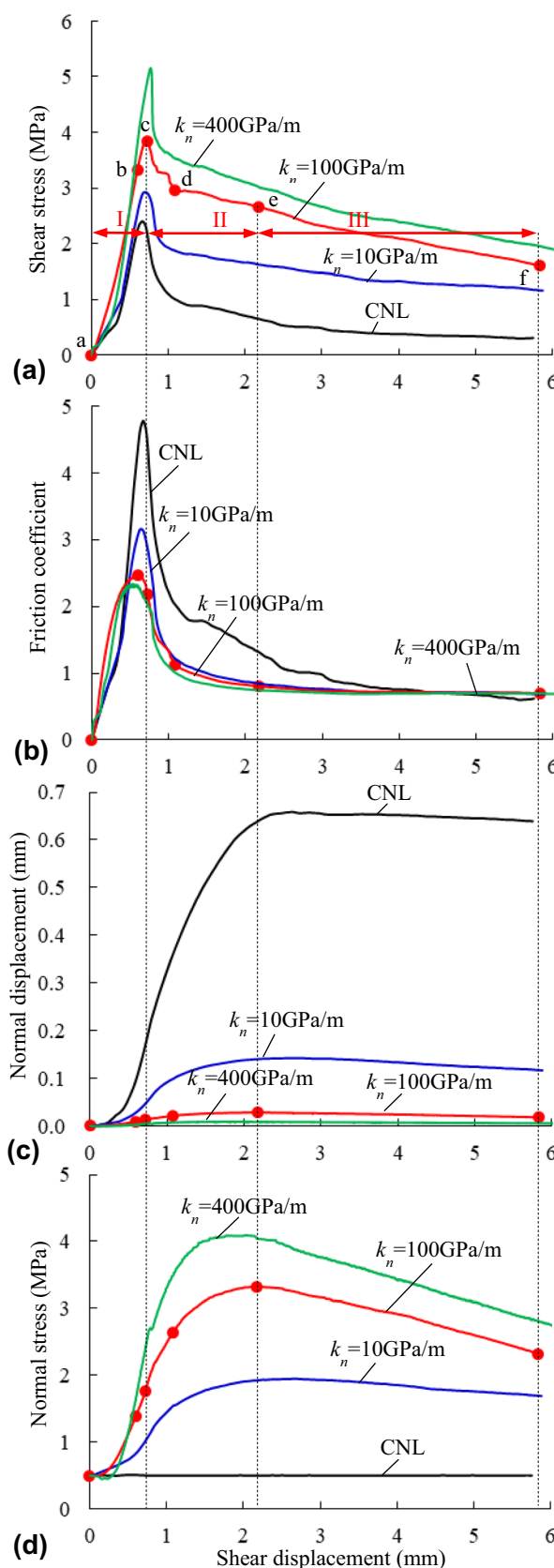
$$\sigma = 401.17v + 0.52(R^2 = 0.99) \tag{3}$$

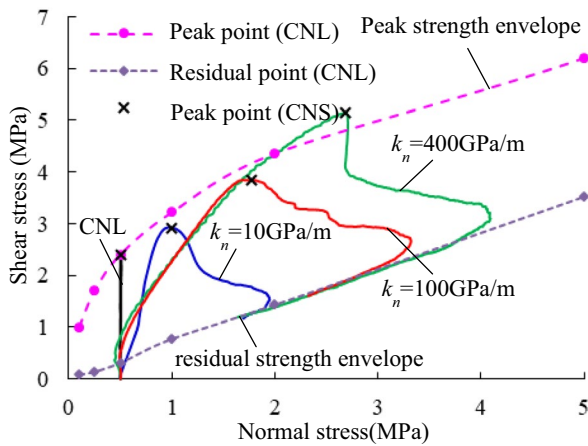
where  $\sigma$  is normal stress,  $v$  is normal displacement, and  $R^2$  is the coefficient of determination of the fitting curves.

The fitting results suggest that the applied normal stiffness and initial normal stress on the bolt–grout interface are nearly equal to the input values of them prior to loading. This confirms that the accuracy of the applied boundary conditions during the shearing process and reliability of the test results are acceptable.

Figure 4 compares the shear behaviors of the bolt–grout interface under the CNL ( $\sigma_{n0}=0.5$  MPa,  $k_n=0$  GPa/m) and CNS ( $\sigma_{n0}=0.5$  MPa,  $k_n=10, 100$  and  $400$  GPa/m) conditions. From Fig. 4a, it can be seen that the shape of shear stress curves is almost the same under both CNL and CNS tests for the range of tested parameters with the following three stages: quasi-elastic stage, strain-softening stage, and friction-sliding stage. The curves of friction coefficient, normal displacement, and normal stress also exhibited similar stage characteristics (see Fig. 4b–d). The friction coefficient refers to the shear stress over normal stress in this study and indicates the relative shearing resistance (Poturovic et al. 2015). Six threshold points (indicated by the solid red circles) are also marked in Fig. 4 for exhibiting the shear behaviors between the bolt and grout material, i.e., test starting point (Point a), peak friction coefficient point (Point b), peak shear stress point (Point c), wear initiation point (Point d), residual friction coefficient initiation point (Point e) and test endpoint (Point f).

A comparison of Fig. 4a–d infers that there is a strong correlation between the shear stress, friction coefficient, normal displacement, and normal stress versus the shear displacement. In the pre-peak quasi-elastic stage, the normal displacement showed a gradually increasing trend, and the shear stress almost increased linearly until approaching Point c. However, the evolution of the friction coefficient depended on the normal boundary conditions. Under the CNL conditions, the friction coefficient showed the same trend as the shear stress did. Under the CNS conditions, the friction coefficient first increased to the peak friction





**Fig. 5** Peak and residual shear strength envelopes in the CNL tests and shear stress—normal stress paths of the bolt–grout interface under the initial normal stress of 0.5 MPa and normal stiffnesses of 0, 10, 100, and 400 GPa/m

coefficient Point b and then decreased to Point c. The results indicated that the peak shear stress point generally lagged behind the peak friction coefficient point in the CNS test. This is because higher normal stress would result in a reduction in the peak friction coefficient and an increase in the shear strength. Followed by the post-peak strain-softening stage, which can be further divided into two small stages according to the decreasing rate of shear stress, i.e., brittle drop stage (Point c to d) and wear stage (Point d to e). In the brittle drop stage, the normal displacement accumulated rapidly, and the shear stress curves displayed a brittle behavior where a sharp drop in the shear stress and friction coefficient was observed after Point c. Besides, the degree of brittleness gradually diminished with the increase of the normal stiffness. Afterward, the normal displacement approached the peak normal displacement point, and the shear stress and the friction coefficient decreased slowly to the residual value in the wear stage. Generally, the peak normal displacement point approximately corresponded to Point e, which was the initiation of the residual friction coefficient representing the onset of completely asperity shearing. In addition, the residual friction coefficient can be obtained at a smaller shear displacement in the CNS tests than that in the CNL tests. Finally, in the friction-sliding stage, friction coefficient remained stable and normal displacement declined slowly. The reduction in the normal displacement is because the sheared-off grout asperity was ground smooth with further shear displacement (Meng et al. 2017), resulting in a reduction in the normal stress applied on the interface and corresponding shear stress in the CNS tests.

Figure 4b depicts the friction coefficient versus shear displacement curves under different normal stiffness conditions. The results indicate that the normal stiffness has

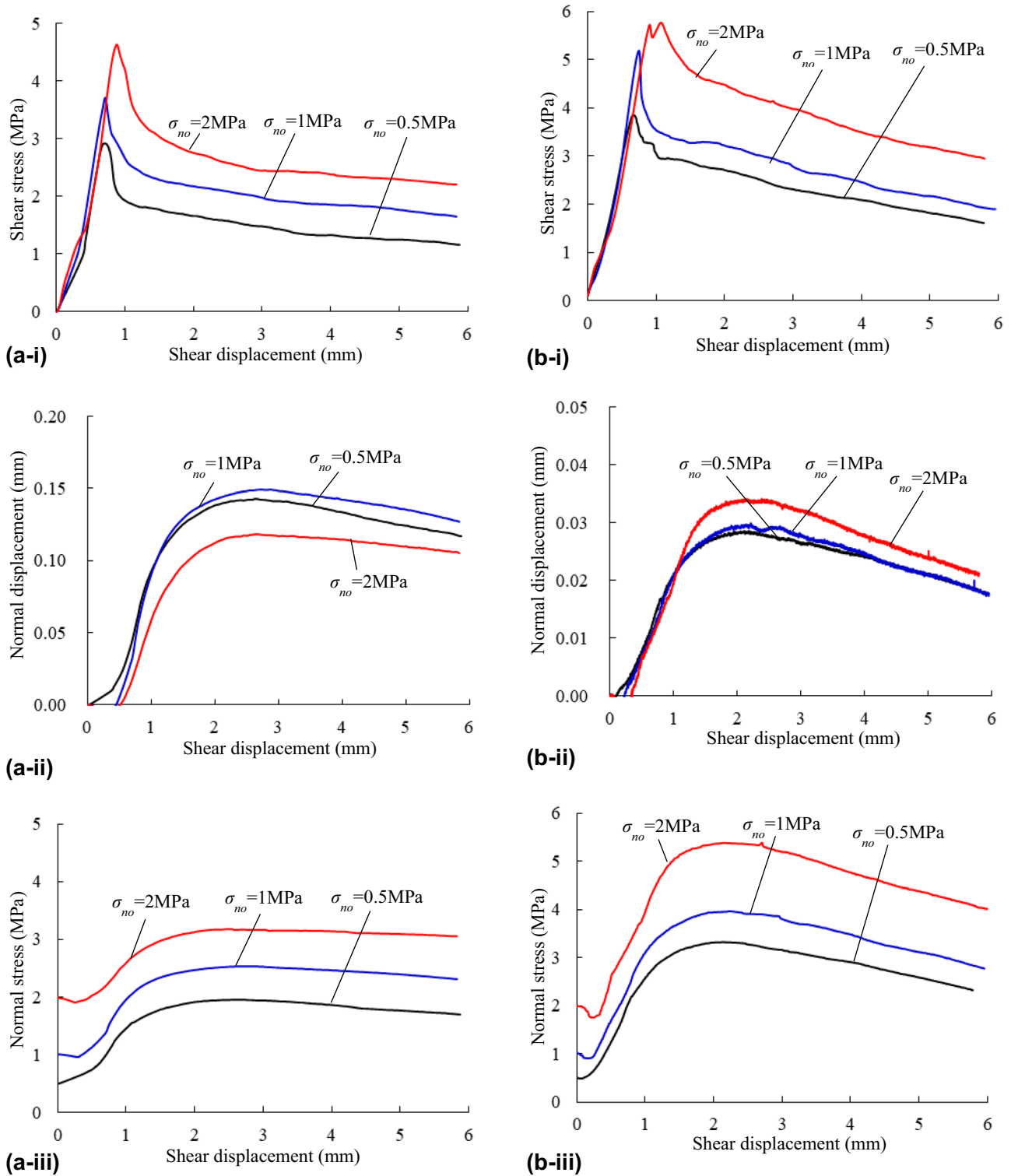
a sound influence on the peak friction coefficient, but it barely influences the residual friction coefficient.

Figure 4c, d depicts the normal displacement and normal stress versus shear displacement curves. Because the change in the normal stress is proportional to the change in the normal displacement under the CNS conditions, the shape of normal displacement and normal stress curves is the same. The normal displacement in the CNS test is far less than that in the CNL test, on the contrary, the normal stress in the CNS test is greater than that in the CNL test. With the increase of normal stiffness, the normal displacement decreased, while the normal stress increased.

Figure 5 illustrates the shear stress versus normal stress paths of the bolt–grout interface under both CNL and CNS conditions. The peak and residual shear strength envelopes of the bolt–grout interface under CNL condition are also presented in the same figure for comparison purpose. Under the CNL condition, stress path varied vertically due to the presence of constant normal stress. The shear stress first increased from 0 to the peak shear strength and then declined to the residual shear strength. Compared with CNL conditions, the stress path is more complicated under the CNS condition because both shear stress and normal stress changed during shearing. The shear stress first increased to the peak point, accompanied by the increase of normal stress. It can be noted that the peak shear stress points for the CNS tests were located near the nonlinear CNL peak strength envelope. The smaller secant slope of the stress path before the peak point was observed under higher normal stiffness conditions. This is because higher normal stiffness can lead to a more rapid increase in the interface normal stress. After the peak shear stress point was reached, the shear stress decreased while the normal stress continued to increase until the maximum normal stress point. The maximum normal stress point at the stress path approached the residual strength envelope. Eventually, the normal and shear stress decreased simultaneously and the stress path approximately varied along with the linear CNL residual strength envelope.

To understand the effect of the initial normal stress on the shear behavior of the bolt–grout interface, three different initial normal stresses (i.e., 0.5, 1 and 2 MPa) were applied on the bolt–grout interface. The test results are shown in Fig. 6. It is clear that the initial normal stress also influences the shear behavior of the bolt–grout interface. A higher initial normal stress generally resulted in a smaller normal deformation and a higher shear strength. The shear stiffness captured in the shear stress curves was almost constant under different initial normal stress levels, and therefore the shear displacement corresponding to the peak shear stress was likely to increase when the initial normal stress was increased. The characteristics of the curves of shear stress, normal displacement, and normal





**Fig. 6** Effects of the initial normal stress on shear behaviors of the bolt–grout interface under the normal stiffnesses of 10 GPa/m (a) and 100 GPa/m (b): (i) shear stress versus shear displacement curves; (ii)

normal displacement versus shear displacement curves; and (iii) normal stress versus shear displacement curves

stress under different initial normal stress conditions were similar.

### 3.2 Analysis of Shear Parameters

The effects of initial normal stress and normal stiffness on the peak and ultimate shear parameters are shown in Fig. 7. The peak shear parameters are defined as the shear parameters corresponding to the peak shear strength and the ultimate shear parameters refer to as the respective maximum value obtained from the direct shear tests. The peak shear strength coincided with the ultimate shear strength in the CNL tests according to the definition.

Figure 7a presents the variation of the peak shear strength with the normal stiffness under different initial normal stress conditions. The peak shear strength showed an increasing trend with the increases of both normal stiffness and initial normal stress. It can also be observed that the effect of the normal stiffness is more pronounced when initial normal stress is small (e.g., 0.5 MPa). As more asperity damages were generated in grout specimens under high initial normal stress conditions, the normal displacement could be suppressed, resulting in a smaller increase of normal stress on the bolt–grout interface under the CNS conditions.

Figure 7b, c illustrates the variations of the peak normal displacement and the ultimate normal displacement with the normal stiffness under different initial normal stress conditions, respectively. Both the peak and ultimate normal displacements generally showed a decreasing trend as the normal stiffness increased. Compared with the ultimate normal displacement obtained from dilation curves, it shows that the peak normal displacement is smaller. In addition, the effect of initial normal stress on the peak and ultimate normal displacement can almost be ignored in the CNS tests. The difference between the peak and ultimate normal displacement is large in the CNL tests and decreased with the increase of normal stiffness in the CNS tests.

Figure 7d, e illustrates the variations of the peak normal stress and the ultimate normal stress with the normal stiffness under different initial normal stress conditions, respectively. Both the peak and ultimate normal stress showed an increasing trend with the increases of normal stiffness and initial normal stress. The ultimate normal stress is larger than the peak normal stress.

Figure 7f, g shows the variation of the peak and the ultimate friction coefficient with the normal stiffness (0–400 GPa/m) at the initial normal stresses of 0.5–2 MPa. The results demonstrated that both the peak and ultimate friction coefficients showed decreasing trends with the increase of the initial normal stress and normal stiffness. The decreasing rate decreased with increasing normal stiffness. Apparently, the peak friction coefficient is slightly smaller than the ultimate friction coefficient. The ultimate friction coefficient is

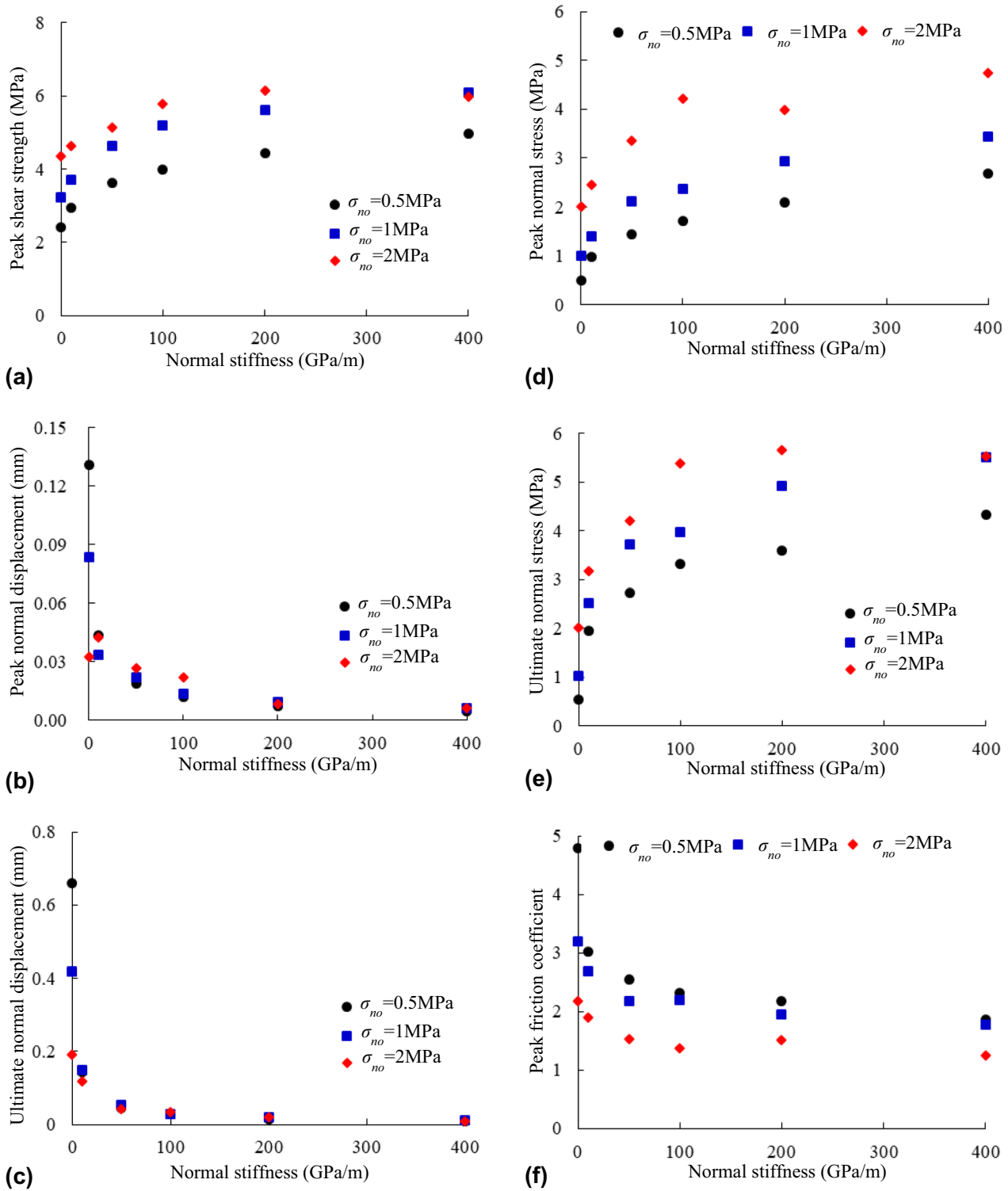
equal to the tangent of the sum of the residual friction angle and the peak dilatancy angle (Maksimović 1992). According to the test results, the residual friction coefficient under different normal stiffnesses is approximately equal (Fig. 4). So, the changing trend of the peak dilatancy angle and the ultimate friction coefficient should be consistent.

The relationship between the shear stress and normal stress at the peak point on the stress paths is shown in Fig. 8. The nonlinear strength envelope of the bolt–grout interface under the CNL conditions is also displayed in the same figure. The results demonstrated that the peak points under the CNS conditions are always located near the CNL strength envelope. At the initial normal stress of 0.5 MPa, the peak shear strength under the CNS conditions is slightly less than that with the same normal stress under the CNL conditions when normal stiffness is between 10 and 100 GPa/m; while they are nearly equal when normal stiffness is larger than 100 GPa/m. However, the peak shear strength under the CNS conditions are generally not less than that with the same peak normal stress under the CNL conditions at the initial normal stresses of 1 and 2 MPa regardless of the normal stiffness. This scenario may be attributed to the fact that the shear behavior of a rock joint is dependent of the stress history (Thirukumaran and Indraratna 2016). In other words, the initial damages resulted from dilational slip failure at initial normal stress of 0.5 MPa, which caused a reduction in the peak shear strength, diminished as normal stiffness increased.

### 3.3 Failure Modes

The failure modes of the bolt–grout interface are shown in Table 3. In this table, it can be observed that the failure modes depended on the applied boundary conditions. Three interface failure modes, i.e., dilational slip failure mode, sheared-off failure mode, and combined failure mode, were identified in this study according to the test results. This observation is similar to that made by Cao et al. (2013).

Under the CNL conditions, these three types of failure modes can be observed, depending on the normal stress. When the initial normal stress is low, e.g., 0.25 MPa, a set of approximately parallel inclined failure surfaces was generated in the grout asperities, causing the grout specimen to ride up and over the steel plate. Hence, the dilational slip failure is a dominant failure mode accompanied by a few sheared-off grout asperities. When the initial normal stress is 2 MPa, the grout asperities were sheared horizontally along the rib base, and the sheared-off failure mode is the main failure mode. When the initial normal stress is between 0.25 MPa and 2 MPa, two types of failure modes coexisted. The generated dilational slip failure surfaces gradually diminished and sheared-off grout asperities gradually increased. This suggests that the interface failure modes



**Fig. 7** Variation of the peak and ultimate shear parameters with the normal stiffness at the initial normal stress of 0.5, 1, and 2 MPa in the CNL and CNS tests: **a** peak shear strength; **b** peak normal displacement;

**c** ultimate normal displacement; **d** peak normal stress; **e** ultimate normal stress; **f** peak friction coefficient; and **g** ultimate friction coefficient

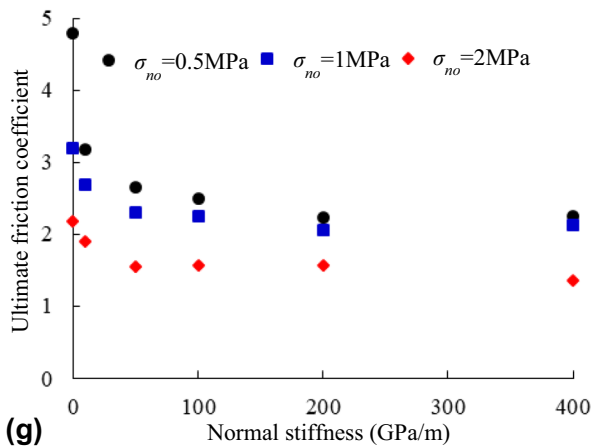
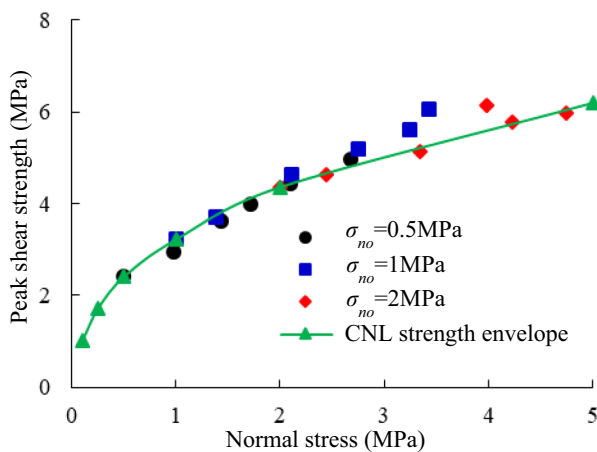


Fig. 7 (continued)



**Fig. 8** Shear stress versus normal stress at the peak point for bolt-grout interface under the CNS conditions and CNL shear strength envelope

transfer from dilational slip failure mode to sheared-off failure mode with the increase of the initial normal stress.

However, only the last two types of failure modes, i.e., sheared-off failure mode and combined failure mode, were observed under the CNS conditions due to the increasing normal stress on the bolt-grout interface for the range of initial normal stress and normal stiffness studied. When both the initial normal stress and normal stiffness are low (e.g.,  $\sigma_{no}=0.5$  MPa,  $K_n=10$  GPa/m), the combined failure mode occurred where the dilational slip failure was first noted at the initial shear stage, similar to that under the same normal stress in the CNL tests, and then the grout asperities were sheared off. With the increase of normal stiffness or initial normal stress, the sheared-off failure mode gradually dominated the interface failure. Sheared-off failure mode under the CNL and CNS conditions is similar. However, a comparison of sheared-off failure modes under different boundary

conditions indicates that scratches were more sound under the CNS conditions.

### 3.4 AE Characteristics

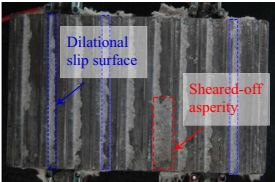
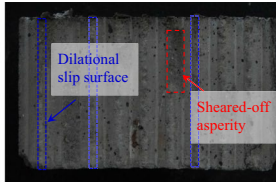
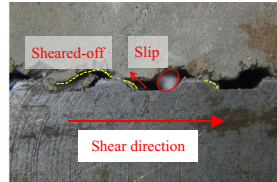
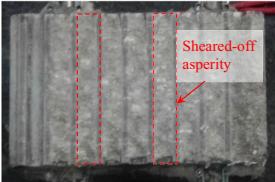

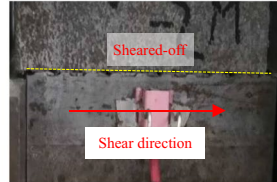


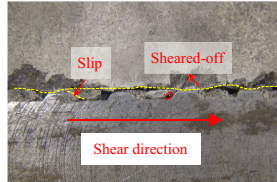
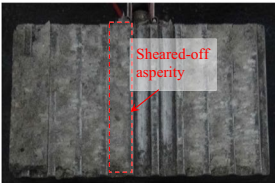
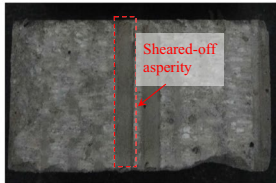
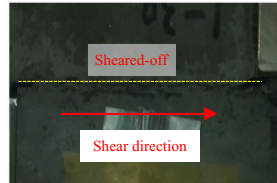
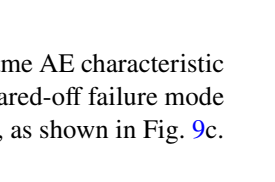
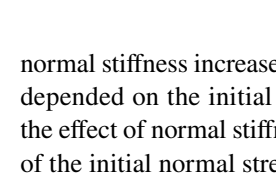
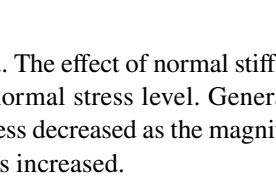
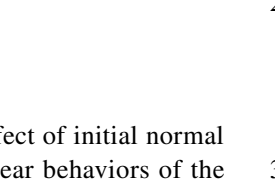
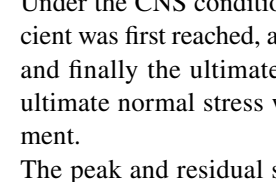
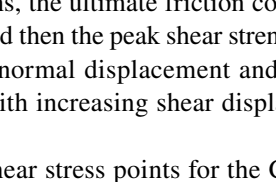
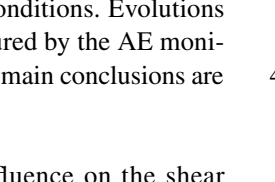
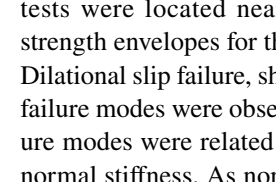
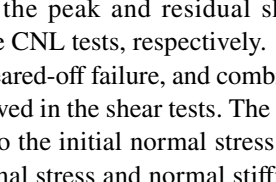
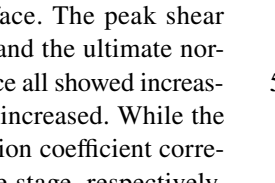
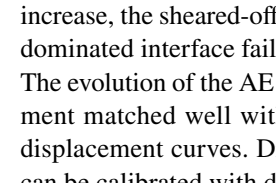
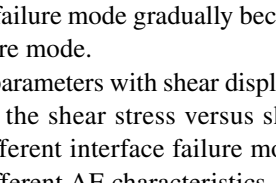
AE parameters were recorded simultaneously during the shearing process to evaluate the interfacial damage process. The typical results of variations of the AE parameters for three types of interface failure modes are shown in Fig. 9. The corresponding shear stress versus shear displacement curve is also illustrated in this figure to investigate the AE characteristics at different deformation stages. The test results revealed that the failure mode of the bolt-grout interface influenced the corresponding AE characteristics. Interestingly, the evolutions of AE parameters matched well with the shear stress curves.

Figure 9a depicts the AE energy rate and the accumulated AE energy rate versus shear displacement curves under the normal stress of 0.25 MPa, where the dilational slip failure occurred. In the pre-peak quasi-elastic shear deformation stage (Stage I), the AE signals were rather quiet concerning low AE energy rate. However, some minor AE energy peaks were noted, which was associated with the generation of the dilational slip surfaces. When shear stress approached the peak shear strength (about 0.9 times the peak shear strength), the AE energy rate increased significantly. Generally, the accumulated AE energy rate was almost negligible in this stage. In the post-peak strain-softening shear deformation stage (Stage II), the AE signals were extremely active and the peak energy rate was observed. The accumulated AE energy rate increased monotonously. In the residual shear stage (Stage III), the AE energy rate rapidly diminished to approximately 0 and then remained almost stable with further shear displacement increment, accompanied by some minor peaks. Therefore, the accumulated AE energy rate was also almost constant for the dilational slip failure mode.

Figure 9b depicts the AE energy rate and accumulated AE energy rate versus shear displacement curves under the normal stress of 2 MPa and normal stiffness of 10 GPa/m where the sheared-off failure occurred. In Stage I, the AE energy and the accumulated energy rate were smaller compared with those in the dilational slip failure mode (see Fig. 9a). In Stage II, the AE energy rate first increased rapidly to the peak AE energy rate and then decreased slowly. The peak energy rate almost matched the turning point from brittle drop stage to wear stage. The accumulated AE energy rate increased rapidly. In Stage III, the AE energy rate resulting from the sliding friction of the sheared-off grout asperities decreased gradually. After that, the accumulated AE energy continued to increase with increasing shear displacement.

For the combined failure mode of the interface under the CNS conditions, the dilational slip failure occurred before the peak and the sheared-off failure occurred mainly after

**Table 3** Typical photos of bolt–grout interfaces with different failure modes after direct shear test

Dominated failure Modes	Boundary conditions	Typical photos of bolt-grout interfaces after direct shear test		
Dilational slip failure	CNL ( $\sigma_{no}=0.5\text{MPa}$ )			
				
Sheared-off failure	CNL ( $\sigma_{no}=2\text{MPa}$ )			
				
Combined failure	CNS ( $\sigma_{no}=0.5\text{MPa}$ , $K_n=10\text{GPa/m}$ )			
				
Sheared-off failure	CNS ( $\sigma_{no}=2\text{MPa}$ , $K_n=10\text{GPa/m}$ )			
				

the peak. Therefore, it displayed the same AE characteristic as dilational slip failure mode and sheared-off failure mode before and after the peak, respectively, as shown in Fig. 9c.

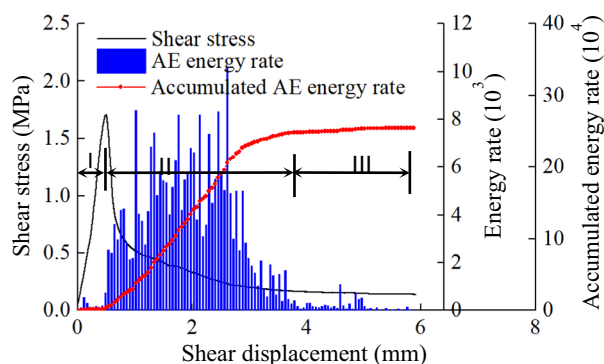
### 4 Conclusions

The present study investigated the effect of initial normal stress and normal stiffness on the shear behaviors of the bolt–grout interface under the CNS conditions. Evolutions of the shear failure process were captured by the AE monitor and digital camera technology. The main conclusions are drawn as follows:

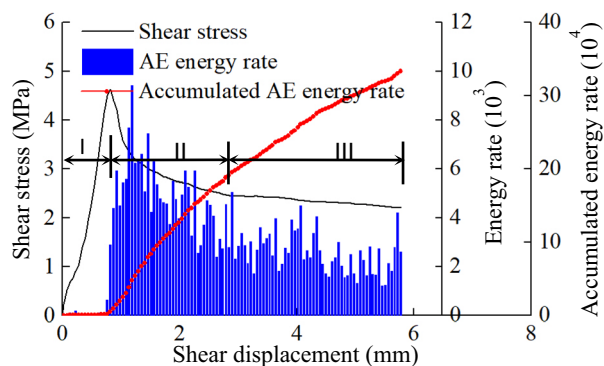
1. Normal stiffness has a major influence on the shear behavior of the bolt–grout interface. The peak shear strength, the peak normal stress, and the ultimate normal stress of the bolt–grout interface all showed increasing trends as the normal stiffness increased. While the normal displacement and the friction coefficient corresponding to the peak and ultimate stage, respectively, showed the opposite change trends, which decreased as

normal stiffness increased. The effect of normal stiffness depended on the initial normal stress level. Generally, the effect of normal stiffness decreased as the magnitude of the initial normal stress increased.

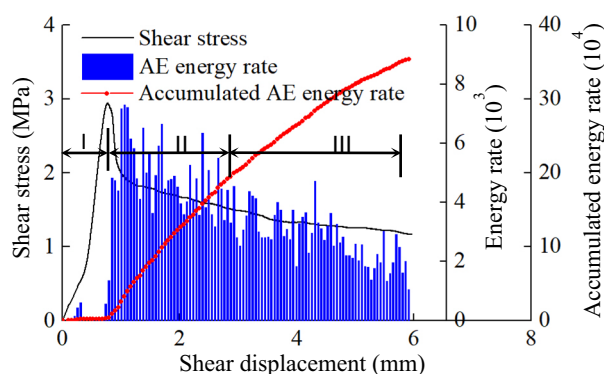
2. Under the CNS conditions, the ultimate friction coefficient was first reached, and then the peak shear strength, and finally the ultimate normal displacement and the ultimate normal stress with increasing shear displacement.
3. The peak and residual shear stress points for the CNS tests were located near the peak and residual shear strength envelopes for the CNL tests, respectively.
4. Dilational slip failure, sheared-off failure, and combined failure modes were observed in the shear tests. The failure modes were related to the initial normal stress and normal stiffness. As normal stress and normal stiffness increase, the sheared-off failure mode gradually became dominated interface failure mode.
5. The evolution of the AE parameters with shear displacement matched well with the shear stress versus shear displacement curves. Different interface failure modes can be calibrated with different AE characteristics.



(a) Dilatational slip failure mode



(b) Sheared-off failure mode



(c) Combined failure mode

**Fig. 9** Evolutions of shear stress, AE energy rate, and accumulated AE energy rate with shear displacement for the bolt–grout interface in the direct shear tests with the following initial load conditions: **a** initial normal stress of 0.25 MPa; **b** initial normal stress of 2 MPa and normal stiffness of 10 GPa/m; and **c** initial normal stress of 0.5 MPa and normal stiffness of 10 GPa/m

**Acknowledgements** This work is supported by the Key projects of the Yalong River Joint Fund of the National Natural Science Foundation of China (U1865203) and the National Natural Science Foundation

of China (51279201). The partial support from the Youth Innovation Promotion Association CAS is gratefully acknowledged.

## Compliance with Ethical Standards

**Conflict of interest** The proper acknowledgments to other works have been given. All of the authors that appear on the submission declare no conflict of interests in the submitted manuscripts and consent to submit. And they have contributed significantly to the work submitted.

## References

- Aziz N, Dey A, Indraratna B (2001) New approach to study load transfer mechanisms of fully grouted bolts. In: Proceedings of 17th international mining congress and exhibition in Turkey, the chamber of mining engineers of turkey. Ankara, pp 143–154
- Aziz N, Jalalifar H, Remennikov AM, Sinclair S, Green A (2008) Optimisation of the bolt profile configuration for load transfer enhancement. In: Coal operators' conference. Wollongong, pp 125–131
- Aziz N, Mirza A, Nemick J (2016) Load transfer characteristics of plain and spiral cable bolts tested in new non rotating pull testing apparatus. In: Coal operators' conference. Wollongong, pp 32–39
- Benmokrane B, Mouchaorab KS, Ballivy G (1994) Laboratory investigation of shaft resistance of rock-socketed piers using the constant normal stiffness direct shear test. *Can Geotech J* 31(3):407–419
- Cai Y, Jiang YJ, Esaki T (2004) A study of rock bolting design in soft rock. *Int J Rock Mech Min Sci* 41(3):1–6
- Cao C (2013) Bolt profile configuration and load transfer capacity optimisation. Ph.D. Dissertation, University of Wollongong
- Cao C, Ren T, Cook C (2013) Calculation of the effect of Poisson's ratio in laboratory push and pull testing of resin-encapsulated bolts. *Int J Rock Mech Min Sci* 64:175–180
- Chen JH, Hagan P, Saydam S (2016) Load transfer behavior of fully grouted cable bolts reinforced in weak rocks under tensile loading conditions. *Geotech Test J* 39(2):252–263
- Chen JH, Hagan P, Saydam S (2018) A new laboratory short encapsulation pull test for investigating load transfer behavior of fully grouted cable bolts. *Geotech Test J* 41(3):435–447
- Gu XF, Seidel JP, Haberfield CM (2003) Direct shear test of sandstone-concrete joints. *Int J Geomech* 3(1):21–33
- Hyett AJ, Bawden WF, Reichert RD (1992) The effect of rock mass confinement on the bond strength of fully grouted cable bolts. *Int J Rock Mech Min Sci* 29(5):503–524
- Hyett AJ, Bawden WFF, Macsporrán GRR, Moosavi M (1995) A constitutive law for bond failure of fully-grouted cable bolts using a modified hoek cell. *Int J Rock Mech Min Sci* 32(1):11–36
- Indraratna B, Haque A (2000) Experimental and numerical modeling of shear behaviour of rock joints. In: *GeoEng 2000, An international conference on geotechnical & geological engineering*. Pennsylvania, USA
- Indraratna B, Haque A, Aziz N (1998) Laboratory modelling of shear behaviour of soft joints under constant normal stiffness conditions. *Geotech Geol Eng* 16(1):17–44
- Jalalifar H (2006) A new approach in determining the load transfer mechanism in fully grouted bolts. Ph.D. Dissertation, University of Wollongong
- Jiang YJ, Li B, Tanabashi Y (2006) Estimating the relation between surface roughness and mechanical properties of rock joints. *Int J Rock Mech Min Sci* 43(6):837–846

- Jiang YJ, Wu XZ, Wang G, Li SC, Wang Q, Cai Y (2016) Bond strength test methods for the bolt-grout-surrounding rock. 28:1–7. (in Chinese)
- Li CC (2012) Performance of D-bolts under static loading. *Rock Mech Rock Eng* 45(2):183–192
- Li CC, Kristjansson G, Høyen AH (2016) Critical embedment length and bond strength of fully encapsulated rebar rockbolts. *Tunn Undergr Sp Technol* 59:16–23
- Ma SQ, Nemcik J, Aziz N (2013) An analytical model of fully grouted rock bolts subjected to tensile load. *Constr Build Mater* 49:519–526
- Maksimović M (1992) New description of the shear strength for rock joints. *Rock Mech Rock Eng* 25(4):275–284
- Martin LB (2012) Theoretical and experimental study of fully grouted rockbolts and cablebolts under axial loads. Ph.D. Dissertation, Ecole Nationale Supérieure des Mines de Paris
- Meng F, Zhou H, Wang Z, Zhang LM, Kong L, Li SJ, Zhang CQ (2017) Influences of shear history and infilling on the mechanical characteristics and acoustic emissions of joints. *Rock Mech Rock Eng* 50(8):2039–2057
- Moosavi M, Bawden W, Hyett A (2002) Mechanism of bond failure and load distribution along fully grouted cable-bolts. *Min Technol* 111(1):1–12
- Moosavi M, Jafari A, Khosravi A (2005) Bond of cement grouted reinforcing bars under constant radial pressure. *Cem Concr Compos* 27(1):103–109
- Poturovic S, Schubert W, Blümel M (2015) Comparison of constant normal load (CNL) and constant normal stiffness (CNS) direct shear tests. In: *ISRM regional symposium-EUROCK 2015*. International Society for Rock Mechanics, pp 445–450
- Salcher M, Bertuzzi R (2018) Results of pull tests of rock bolts and cable bolts in Sydney sandstone and shale. *Tunn Undergr Sp Technol* 74:60–70
- Seidel JP, Haberfield CM (2002) Laboratory testing of concrete-rock joints in constant normal stiffness direct shear. *Geotech Test J* 25(4):391–404
- Shrivastava AK, Rao KS (2018) Physical modeling of shear behavior of infilled rock joints under CNL and CNS boundary conditions. *Rock Mech Rock Eng* 51(1):101–118
- Stille H, Holmberg M, Nord G (1989) Support of weak rock with grouted bolts and shotcrete. *Int J Rock Mech Min Sci* 26(1):99–113
- Thenevin I, BlancoMartín L, HadjHassen F, Schleifer J, Lubosik Z, Wrana A (2017) Laboratory pull-out tests on fully grouted rock bolts and cable bolts: results and lessons learned. *J Rock Mech Geotech Eng* 9(5):843–855
- Thirukumaran S, Indraratna B (2016) A review of shear strength models for rock joints subjected to constant normal stiffness. *J Rock Mech Geotech Eng* 8(3):405–414
- Villaescusa E, Varden R, Hassell R (2008) Quantifying the performance of resin anchored rock bolts in the Australian underground hard rock mining industry. *Int J Rock Mech Min Sci* 45(1):94–102
- Yokota Y, Zhao ZY, Nie W, Date K, Iwano K, Okada Y (2018) Experimental and numerical study on the interface behaviour between the rock bolt and bond material. *Rock Mech Rock Eng* 52(3):1–11
- Zhang CQ, Cui GJ, Zhou H, Liu LP, Liu ZJ, Lu JJ, Cheng GT (2018) Experimental study on shear and deformation characteristics of the rod-grout interface. *Chin J Rock Mech Eng* 37(4):820–828 (in Chinese)

**Publisher's Note** Springer Nature remains neutral with regard to jurisdictional claims in published maps and institutional affiliations.